ACS APPLIED MATERIALS & INTERFACES

Research Article

www.acsami.org

Fabrication of Transparent-Conducting-Oxide-Coated Inverse Opals as Mesostructured Architectures for Electrocatalysis Applications: A Case Study with NiO

Vennesa O. Williams,[†,‡,▽] Erica J. DeMarco,[†,‡,▽] Michael J. Katz,[†] Joseph A. Libera,[§] Shannon C. Riha,[‡] Dong Wook Kim,[†] Jason R. Avila,[†] Alex B. F. Martinson,[‡] Jeffrey W. Elam,[§] Michael J. Pellin,[†,‡] Omar K. Farha,*[,†,⊥] and Joseph T. Hupp*[,†,‡,∥]

[†]Department of Chemistry and Argonne-Northwestern Solar Energy Research Center (ANSER), Northwestern University, 2145 Sheridan Road, Evanston, Illinois 60208, United States

[‡]Materials Science Division, Argonne National Laboratory, 9700 S. Cass Avenue, Argonne, Illinois 60439, United States

[§]Energy Systems Division, Argonne National Laboratory, 9700 S. Cass Avenue, Argonne, Illinois 60439, United States

[∥]Chemical Science and Engineering Division, Argonne National Laboratory, 9700 S. Cass Avenue, Argonne, Illinois 60439, United States

[⊥]Department of Chemistry, Faculty of Science, King Abdulaziz University, Jeddah, Saudi Arabia

Supporting Information

ABSTRACT: Highly ordered, and conductive inverse opal arrays were made with silica and subsequently coated with tin-doped indium oxide (ITO) via atomic layer deposition (ALD). We demonstrate the utility of the resulting mesostructured electrodes by further coating them with nickel oxide via ALD. The NiO-coated arrays are capable of efficiently electrochemically evolving oxygen from water. These modular, crack-free, transparent, high surface area, and conducting structures show promise for many applications including electrocatalysis, photocatalysis, and dye-sensitized solar cells.

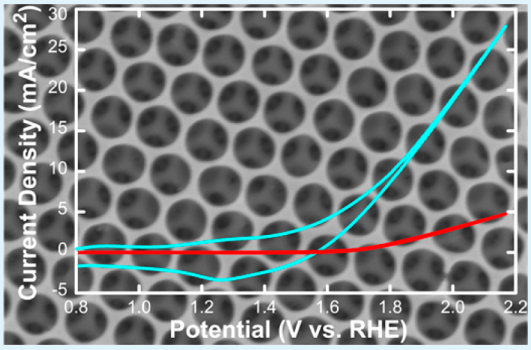

KEYWORDS: *nickel oxide, water oxidation, atomic-layer deposition, inverse opals, catalysis, electrochemistry*

INTRODUCTION

Previous work has demonstrated that high-surface-area architectures are well-positioned to address several key challenges in photoelectrochemical solar-energy conversion.[1−9] For example, high-surface-area silica-based aerogels can be used as scaffolds for constructing quasi-one-dimensional photoelectrodes that, when deployed in dye-sensitized solar cells (DSCs), display both good light-harvesting and good charge collection.[5−7,10] Since SiO_2 aerogels are insulating, electrode fabrication was accomplished by conformally coating the SiO_2 with ZnO, TiO_2, or both, via atomic-layer deposition (ALD); the advantage of this protocol is that it is not necessary to devise ways of making high-surface-area electrodes (e.g., aerogels) directly from conducting materials (e.g., fluorine-doped tin oxide, or tin-doped indium oxide (ITO)). This approach converts convenient but electrochemically inert scaffolds into functional structures using a two-step procedure—namely, making the high-surface-area architecture, which can constitute any of a broad range of materials, and then coating it with the desired metal oxide.[11,12] Consequently, this approach has been applied to various high-surface-area materials, including aerogels,[5−7,10,13−15] sintered nanoparticles,[16,17] and anodic aluminum oxide.[9,18−22]

Among the several types of high-surface-area materials, inverse opals (IOs) are attractive because they are easily fabricated, stable, and because they offer large void fractions.[23−26,16] A scanning electron microscopy (SEM) image of an IO prepared in our laboratories is shown in Figure 1 (top). Since IOs can be fabricated from readily available, monodispersed polystyrene (PS) spheres in a variety of sizes, the apertures shown in the figure can be easily tuned to adjust the porosity for a desired application. Furthermore, by changing the concentration of polystyrene spheres, the number of layers (i.e., thickness) of the IO can be easily tuned. Depending on the application, it is sometimes desirable that IOs and IO-derived assemblies be crack-free. Most methods of IO fabrication produce structures containing significant numbers of cracks and other inhomogeneities—consequences of the

Received: March 28, 2014
Accepted: July 9, 2014
Published: July 17, 2014

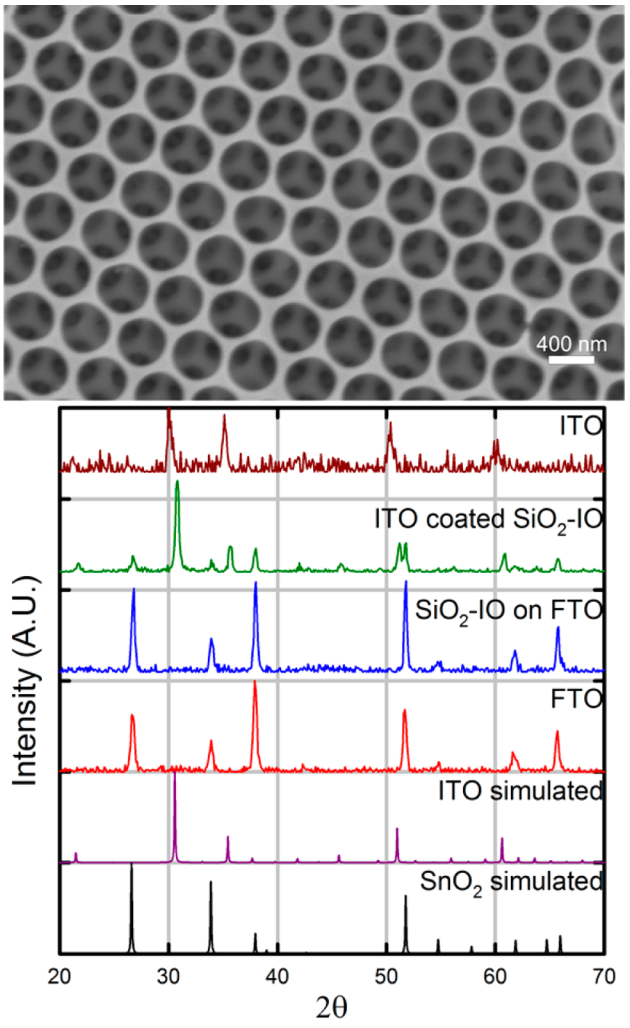

Figure 1. (Top) SEM image of a SiO_2 inverse opal. (Bottom) Observed and simulated powder X-ray diffraction (XRD) diffractograms of the systems presented herein.[31−33]

infiltration technique utilized. However, Hatton et al. have nicely solved this problem by co-depositing the precursor of the IO material with the templating PS spheres.[24] Herein, we employ this strategy, together with ALD, to obtain ordered, crack-free, transparent, and conductive IO electrodes.[27] To illustrate the utility of this architecture, we further coat the conducting electrodes with nickel oxide and explore their behavior as electrocatalysts for oxygen evolution in alkaline water.

RESULTS AND DISCUSSION

IOs were fabricated on planar, fluorine-doped tin oxide (FTO)-coated glass platforms (Figure 1 (top)).[24] As illustrated by Hatton et al.,[24] our films were crack-free over the entirety of the film (Figure S1 in the Supporting Information (SI) confirms the crack-free nature of the film over a ca. 40 μm wide section). X-ray diffraction (XRD) diffractograms of the bare FTO-coated glass and one coated with a silica IO (Figure 1 (bottom)) suggest that the IOs are not crystalline. Utilizing ALD, the insulating IO scaffold was conformally coated with tin-doped indium oxide (ITO).[28−30] Figure 1 (bottom) shows XRD diffractograms of both ITO-coated inverse opals (ITO-IO) and ITO-coated glass; the diffraction peaks of ITO can be observed in both XRD diffractograms,[31] confirming the successful coating of the IO framework. Figure S4 in the SI illustrates the conformal distribution of both tin and indium of the ITO-coated IO framework.

To estimate the enhancement in solution-accessible surface area for the opal structure relative to a flat electrode, we exposed both types of electrodes to an ethanol solution of a high-extinction dye (a tetraphenyl-carboxylated porphyrin; see the SI), and then thoroughly rinsed the electrodes. We then removed the adsorbed dye molecules from the electrodes by immersion in basic ethanol. From subsequently electronic absorption spectra of the solutions, we determined the amounts adsorbed.[5] From the ratio of amounts adsorbed, we obtained an estimate of 50 for the enhancement in electrode surface area due to the opal architecture (see Figure S3 in the SI). This result is in good agreement with a value of 65 derived from a simplified geometric model of a six-layer opal electrode (see the SI).[26] Furthermore, CO curves of flat ITO vs ITO-coated IO frameworks (see Figure S2 in the SI) demonstrate a significantly higher current for the Sn(II)/Sn(IV) redox wave for the IO electrode. This is indicative of the fact that more than just the outermost portion of the IO framework is electrochemically active.

To demonstrate the utility of the ITO-IO arrays, we further deposited NiO via ALD atop the ITO-coated IO array (Figure S5 in the SI).[34] NiO is a *p*-type semiconductor; it has been widely applied for *p*-type dye-sensitized solar cells (DSSCs) due to its reasonably favorable valence band position,[35−37] electrochromic materials due to the color change associated with the Ni(II)/Ni(III) redox couple,[38,39] and its role as an electrochemical catalyst for water oxidation, especially under highly alkaline conditions.[40,41] With the last application in mind, NiO was deposited by ALD onto ITO-IO frameworks offering surface areas ca. 50 times greater than the geometric area. Elemental mapping of a representative NiO-coated ITO-IO array via energy-dispersive X-ray (EDX) analysis showed that Ni is uniformly distributed (see Figure S5 in the SI). Figure 2 shows cyclic voltammograms for a NiO-coated ITO-IO electrode and a flat NiO electrode in aqueous 1 M NaOH. Compared to the flat NiO electrode, an enhancement in

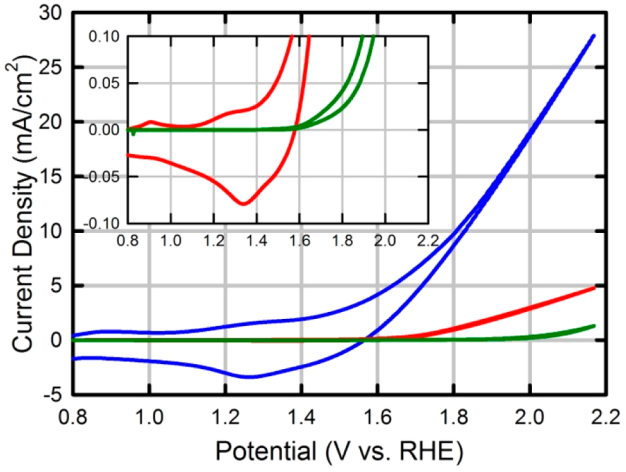

Figure 2. Cyclic voltammograms at 25 mV/s for 16-nm NiO-coated ITO-IO (blue), 16-nm NiO flat (red), and flat ITO (green) in 1 M NaOH; inset shows an expanded scale for flat NiO and for ITO. Note the appearance, for the former, of a pair of surface redox peaks near 1.3 V.

catalytic current density (*vide infra*) and a decreased onset potential can be observed in the CV curve of the NiO-coated ITO-IO electrode. Interestingly, on flat electrodes, the thickness of the NiO film did not significantly affect the water oxidation performance (Figure S6 in the SI). Similarly, they did not significantly change the magnitude of the Ni(II/III) wave near 1.30 V. These results imply that only the outermost portion of the NiO film is catalytically active. This behavior differs from that for films prepared by methods such as electrodeposition or electro-oxidation of metallic nickel, where current due to oxygen evolution scales with the amount of oxidized nickel present.[42] The confinement of electrocatalytic activity to the outermost part of the ALD-prepared film is ascribed to an inability of OH^- to permeate NiO. In contrast to ALD-derived NiO, the oxidized nickel-containing films obtained via other methods are typically described as hydroxides or oxyhydroxides.

To gain insight into the mechanism of water electro-oxidation, the dependence of current density for water oxidation on applied electrode potential was examined.[43] After cycling the films several times between −0.5 V and 1.5 V vs Ag/AgCl, a Tafel slope (i.e., slope of a plot of electrode potential against the log of the current density) of 60 mV/decade was observed at pH 13 and pH 14. (Accurate assessment required minimization of cell resistance and correction for remaining cell resistance, i.e., correction for *iR* contributions to the measured potential. Needed resistance values were collected via impedance measurements.) This slope indicates that (i) one of the four required holes are transferred before the rate-determining step, and (ii) the rate-controlling step is chemical rather than electrochemical.[43] Depending on the details of oxide (hydroxide) preparation, other studies have yielded Tafel slopes of ca. 60, 40, or 30 mV/decade.[40,44−47]

Assessment of the pH dependence of the rate of oxidation (i.e., current density) at fixed potential versus a pH-independent reference electrode yields a reaction order of −2 in H^+, or, equivalently, +2 in OH^-.

Electrochemical conditioning of NiO films has been shown to improve catalytic activity via *in situ* formation of $Ni(OH)_2$/NiOOH species.[40,42,45,46] The layered structure of NiOOH, which forms upon conditioning, allows for more of the Ni atoms to be electrochemically accessible.[40] Galvanostatic conditioning of an ALD-grown NiO-ITO electrode on an IO support for 6 h at 10 mA/cm^2 yielded ca. 2-fold increase in catalytic current at fixed overpotential (Figure S7 in the SI). Accompanying the enhanced catalytic activity (diminished reaction overpotential) was a ca. 1.5-fold increase in the current observed for reversible oxidation of Ni(II) to Ni(III) in cyclic voltammetry experiments (initial NiO coating thickness = 21 nm).

Finally, to facilitate eventual comparisons to other electrodes in water oxidation experiments, we determined the overpotential necessary to generate 10 mA/cm^2. At pH 14, ca. 400 mV (uncorrected for cell resistance)/300 mV (corrected for 40 Ω cell resistance) of overpotential (subsequent to galvanostatic conditioning) was required; this value is similar to values reported for other nickel-oxide (hydroxide)-based water oxidation electrocatalysts in alkaline solution.[40]

CONCLUSIONS

In summary, we find that high-surface-area, crack-free electrodes can be conveniently obtained by preparing silica inverse opals (IOs) on conductive glass platforms and then conformally overcoating the IO structures with a few tens of nanometers of indium tin oxide (ITO) via atomic-layer deposition. Relative to flat electrodes, the new electrodes display ca. 1.8 orders of magnitude greater elecroactivity as indicated, for example, by charging currents. The increase is consistent with expectations based on full utilization of the additional surface area created by adding an IO scaffold to the flat electrode. In principle, enhancements larger or smaller than 1.8 orders of magnitude can be obtainable by varying the thickness of the initial opal-organized templating film of polystyrene spheres or by varying the diameter of the spheres. As a representative potential application, the utility of IO electrodes for water oxidation was examined. To render the high-area electrodes catalytic for this reaction, they were coated with nickel oxide, again via ALD. The coated electrodes indeed exhibit electrocatalytic activity and the current densities are consistent with the enhanced surface area. Current efforts are focused on employing similar structures as *p*-type electrodes and distributed current-collectors in dye-sensitized solar cells.

EXPERIMENTAL SECTION

Unless noted otherwise, chemicals were purchased from Sigma−Aldrich and were used as received. Tin-doped indium oxide (ITO) was deposited by ALD on cleaned 8 Ω/cm^2 fluorine-doped tin oxide (FTO) supported on 1.5 cm × 1.5 cm glass squares (Hartford Glass) according to a previously reported technique.[28,29] Si(001) witness chips were used to record the deposited film thicknesses.

High-surface-area, crack-free inverse opal (IO) frameworks of silica were constructed according to the method of Hatton et al.[24] In order to efficiently coat the IO framework with ITO, exposure times of 5 s were used for all precursors.[28−30] The IO samples were coated with 21 nm of ITO, as determined by ellipsometry on a Si(001) witness sample.

Nickel oxide was deposited using a proprietary nickel precursor (Dow Electronic Materials AccuDep Nickel precursor) and deionized water.[34] The reactor temperature was 200 °C, and the temperature of the Ni precursor was 130 °C. The Ni precursor was pulsed into the chamber for 2 s and then allowed to react with the sample for 18 s before evacuating the precursor for 60 s. Subsequently, H_2O was pulsed into the reactor for 0.03 s and then held in the chamber for 5 s, before an evacuation of 40 s. Flat films prepared on commercial ITO substrates (Delta Technologies, Ltd.) were also placed in the reaction chamber during deposition. Ellipsometry measurements of NiO growth on ALD-ITO coated silicon witness films indicated a growth rate of 0.7 Å per cycle.

Scanning electron microscopy (SEM) and energy-dispersive X-ray spectroscopy (EDS) images were collected on a Hitachi S-4800-II cFEG SEM. For SEM images, electrodes were sputtered with osmium prior to image capture with an accelerating voltage of 10 kV (increased to 20 kV when using EDS). XRD measurements were done using a Rigaku XDS 2000 diffractometer featuring nickel-filtered Cu Kα radiation (λ = 1.5418 Å). Data were collected over a range of 20° < 2θ < 85° in 0.05° steps with a 2 s counting time per step.

Electrochemical measurements were conducted with a platinum mesh counter electrode and a Ag/AgCl (sat. KCl) reference electrode; data were subsequently adjusted to the reversible hydrogen electrode (RHE) scale. Water oxidation was carried out in a three-electrode cell, using a Solartron Analytical potentiostat. Electrode surface areas (geometric areas) were fixed at 0.25 cm^2 by using Surlyn to cover the remainder of the electrode.

ASSOCIATED CONTENT

Supporting Information

Synthesis of the tetraphenyl-carboxylated porphyrin used for dye-desorption experiments, SEM and energy-dispersive X-ray spectroscopy of ITO-coated electrodes and NiO-coated

electrodes, effect of NiO thickness on the oxygen evolution reaction, effect of electrode conditioning on the oxygen evolution reaction is available in the electronic Supporting Information, and explanation of geometric calculation of surface area increase due to opal architecture. This material is available free of charge via the Internet at http://pubs.acs.org.

AUTHOR INFORMATION

Corresponding Authors

*E-mail: o-farha@northwestern.edu (O. K. Farha).
*E-mail: j-hupp@northwestern.edu (J. T. Hupp).

Author Contributions

[∇]These authors contributed equally.

Notes

The authors declare no competing financial interest.

ACKNOWLEDGMENTS

This work was supported as part of the ANSER Center, an Energy Frontier Research Center funded by the U.S. Department of Energy, Office of Science, Office of Basic Energy Sciences under Award No. DE-SC0001059.

REFERENCES

(1) Law, M.; Greene, L. E.; Johnson, J. C.; Saykally, R.; Yang, P. Nanowire Dye-Sensitized Solar Cells. *Nat. Mater.* **2005**, *4*, 455−459.

(2) Zhang, Q.; Park, K.; Xi, J.; Myers, D.; Cao, G. Recent Progress in Dye-Sensitized Solar Cells Using Nanocrystallite Aggregates. *Adv. Eng. Mater.* **2011**, *1*, 988−1001.

(3) Kowalski, D.; Kim, D.; Schmuki, P. TiO_2 Nanotubes, Nanochannels and Mesosponge: Self-Organized Formation and Applications. *Nano Today* **2013**, *8*, 235−264.

(4) O'Regan, B.; Grätzel, M. A Low-Cost, High-Efficiency Solar Cell Based on Dye-Sensitized Colloidal TiO_2 Films. *Nature* **1991**, *353*, 737−740.

(5) Williams, V. O.; Jeong, N. C.; Prasittichai, C.; Farha, O. K.; Pellin, M. J.; Hupp, J. T. Fast Transporting ZnO−TiO_2 Coaxial Photoanodes for Dye-Sensitized Solar Cells Based on ALD-Modified SiO_2 Aerogel Frameworks. *ACS Nano* **2012**, *6*, 6185−6196.

(6) Hamann, T. W.; Martinson, A. B. F.; Elam, J. W.; Pellin, M. J.; Hupp, J. T. Atomic Layer Deposition of TiO_2 on Aerogel Templates: New Photoanodes for Dye-Sensitized Solar Cells. *J. Phys. Chem. C* **2008**, *112*, 10303−10307.

(7) Hamann, T. W.; Martinson, A. B. F.; Elam, J. W.; Pellin, M. J.; Hupp, J. T. Aerogel Templated ZnO Dye-Sensitized Solar Cells. *Adv. Mater.* **2008**, *20*, 1560−1564.

(8) Martinson, A. B. F.; Hamann, T. W.; Pellin, M. J.; Hupp, J. T. New Architectures for Dye-Sensitized Solar Cells. *Chem.—Eur. J.* **2008**, *14*, 4458−4467.

(9) Martinson, A. B. F.; Elam, J. W.; Liu, J.; Pellin, M. J.; Marks, T. J.; Hupp, J. T. Radial Electron Collection in Dye-Sensitized Solar Cells. *Nano Lett.* **2008**, *8*, 2862−2866.

(10) Li, T. C.; Fabregat-Santiago, F.; Farha, O. K.; Spokoyny, A. M.; Raga, S. R.; Bisquert, J.; Mirkin, C. A.; Marks, T. J.; Hupp, J. T. SiO_2 Aerogel Templated, Porous TiO_2 Photoanodes for Enhanced Performance in Dye-Sensitized Solar Cells Containing a Ni(III)/(IV) Bis(Dicarbollide) Shuttle. *J. Phys. Chem. C* **2011**, *115*, 11257−11264.

(11) Detavernier, C.; Dendooven, J.; Pulinthanathu Sree, S.; Ludwig, K. F.; Martens, J. A. Tailoring Nanoporous Materials by Atomic Layer Deposition. *Chem. Soc. Rev.* **2011**, *40*, 5242−5253.

(12) George, S. M. Atomic Layer Deposition: An Overview. *Chem. Rev.* **2010**, *110*, 111−131.

(13) Mane, A. U.; Greene, J. P.; Nolen, J. A.; Sampathkumaran, U.; Owen, T. W.; Winter, R.; Elam, J. W. Refractory Nanoporous Materials Fabricated Using Tungsten Atomic Layer Deposition on Silica Aerogels. *Appl. Surf. Sci.* **2012**, *258*, 6472−6478.

(14) Korhonen, J. T.; Kettunen, M.; Ras, R. H. A.; Ikkala, O. Hydrophobic Nanocellulose Aerogels as Floating, Sustainable, Reusable, and Recyclable Oil Absorbents. *ACS Appl. Mater. Interfaces* **2011**, *3*, 1813−1816.

(15) Korhonen, J. T.; Hiekkataipale, P.; Malm, J.; Karppinen, M.; Ikkala, O.; Ras, R. H. A. Inorganic Hollow Nanotube Aerogels by Atomic Layer Deposition onto Native Nanocellulose Templates. *ACS Nano* **2011**, *5*, 1967−1974.

(16) Tétreault, N.; Arsenault, E.; Heiniger, L.-P.; Soheilnia, N.; Brillet, J.; Moehl, T.; Zakeeruddin, S.; Ozin, G. A.; Grätzel, M. High-Efficiency Dye-Sensitized Solar Cell with Three-Dimensional Photoanode. *Nano Lett.* **2011**, *11*, 4579−4584.

(17) Prasittichai, C.; Avila, J. R.; Farha, O. K.; Hupp, J. T. Systematic Modulation of Quantum (Electron) Tunneling Behavior by Atomic Layer Deposition on Nanoparticulate SnO_2 and TiO_2 Photoanodes. *J. Am. Chem. Soc.* **2013**, *135*, 16328−16331.

(18) Romero, V.; Vega, V.; García, J.; Zierold, R.; Nielsch, K.; Prida, V. M.; Hernando, B.; Benavente, J. Changes in Morphology and Ionic Transport Induced by ALD SiO_2 Coating of Nanoporous Alumina Membranes. *ACS Appl. Mater. Interfaces* **2013**, *5*, 3556−3564.

(19) Phillips, R.; O'Toole, A.; He, X.; Hansen, R.; Geer, R.; Eisenbraun, E. Processing and Functionalization of Conductive Substoichiometric TiO_2 Catalyst Supports for PEM Fuel Cell Applications. *J. Mater. Res.* **2012**, *28*, 461−467.

(20) Zhang, W.; Qiu, T.; Qu, X.-P.; Chu, P. K. Atomic Layer Deposition of Platinum Thin Films on Anodic Aluminium Oxide Templates as Surface-Enhanced Raman Scattering Substrates. *Vacuum* **2013**, *89*, 257−260.

(21) Chen, X.; Pomerantseva, E.; Banerjee, P.; Gregorczyk, K.; Ghodssi, R.; Rubloff, G. Ozone-Based Atomic Layer Deposition of Crystalline V_2O_5 Films for High Performance Electrochemical Energy Storage. *Chem. Mater.* **2012**, *24*, 1255−1261.

(22) Norek, M.; Łuka, G.; Godlewski, M.; Płociński, T.; Michalska-Domańska, M.; Stępniowski, W. J. Plasmonic Enhancement of Blue Emission from ZnO Nanorods Grown on the Anodic Aluminum Oxide (AAO) Template. *Appl. Phys., A* **2012**, *111*, 265−271.

(23) Stein, A.; Wilson, B. E.; Rudisill, S. G. Design and Functionality of Colloidal-Crystal-Templated Materials—Chemical Applications of Inverse Opals. *Chem. Soc. Rev.* **2013**, *42*, 2763−2803.

(24) Hatton, B.; Mishchenko, L.; Davis, S.; Sandhage, K. H.; Aizenberg, J. Assembly of Large-Area, Highly Ordered, Crack-Free Inverse Opal Films. *Proc. Natl. Acad. Sci. U.S.A.* **2010**, *107*, 10354−10359.

(25) Stein, A.; Li, F.; Denny, N. R. Morphological Control in Colloidal Crystal Templating of Inverse Opals, Hierarchical Structures, and Shaped Particles. *Chem. Mater.* **2008**, *20*, 649−666.

(26) Yang, Z.; Gao, S.; Li, W.; Vlasko-Vlasov, V.; Welp, U.; Kwok, W.-K.; Xu, T. Three-Dimensional Photonic Crystal Fluorinated Tin Oxide (FTO) Electrodes: Synthesis and Optical and Electrical Properties. *ACS Appl. Mater. Interfaces* **2011**, *3*, 1101−1108.

(27) In a recent report on high-area hematite-based photoelectrodes, we used the conductive inverse-opals as scaffolds, but deferred a substantive report to the present paper. See: Riha, S. C.; DeVries Vermeer, M. J.; Pellin, M. J.; Hupp, J. T.; Martinson, A. B. F. Hematite-based Photo-oxidation of Water Using Transparent, Distributed Current-Collectors. *ACS Appl. Mater. Interfaces* **2013**, *5*, 360.

(28) Libera, J. A.; Hryn, J. N.; Elam, J. W. Indium Oxide Atomic Layer Deposition Facilitated by the Synergy between Oxygen and Water. *Chem. Mater.* **2011**, *23*, 2150−2158.

(29) Elam, J. W.; Baker, D. A.; Martinson, A. B. F.; Pellin, M. J.; Hupp, J. T. Atomic Layer Deposition of Indium Tin Oxide Thin Films Using Nonhalogenated Precursors. *J. Phys. Chem. C* **2008**, *112*, 1938−1945.

(30) Elam, J. W.; Baker, D. A.; Hryn, A. J.; Martinson, A. B. F.; Pellin, M. J.; Hupp, J. T. Atomic Layer Deposition of Tin Oxide Films Using Tetrakis(Dimethylamino) Tin. *J. Vac. Sci. Technol. A* **2008**, *26*, 244−252.

(31) Nadaud, N.; Lequeux, N.; Nanot, M.; Jové, J.; Roisnel, T. Structural Studies of Tin-Doped Indium Oxide (ITO) and $In_4Sn_3O_{12}$. *J. Solid State Chem.* **1998**, *135*, 140−148.
(32) Baur, W. H.; Khan, A. A. Rutile-Type Compounds. IV. SiO_2, GeO_2 and a Comparison with Other Rutile-Type Structures. *Acta Crystallogr., Sect. B: Struct. Sci.* **1971**, *27*, 2133−2139.
(33) The difference between the diffraction pattern of ITO and the simulated diffraction pattern of ITO is likely due to slight misalignment of the diffraction beam with respect to the detector (i.e., a zeroshift error).
(34) Thimsen, E.; Martinson, A. B. F.; Elam, J. W.; Pellin, M. J. Energy Levels, Electronic Properties, and Rectification in Ultrathin *p*-NiO Films Synthesized by Atomic Layer Deposition. *J. Phys. Chem. C* **2012**, *116*, 16830−16840.
(35) Gibson, E. A.; Smeigh, A. L.; Le Pleux, L.; Hammarström, L.; Odobel, F.; Boschloo, G.; Hagfeldt, A. Cobalt Polypyridyl-Based Electrolytes for *p*-Type Dye-Sensitized Solar Cells. *J. Phys. Chem. C* **2011**, *115*, 9772−9779.
(36) Odobel, F.; Pellegrin, Y.; Gibson, E. A.; Hagfeldt, A.; Smeigh, A. L.; Hammarström, L. Recent Advances and Future Directions to Optimize the Performances of *p*-Type Dye-Sensitized Solar Cells. *Coord. Chem. Rev.* **2012**, *256*, 2414−2423.
(37) Odobel, F.; Le Pleux, L.; Pellegrin, Y.; Blart, E. New Photovoltaic Devices Based on the Sensitization of *p*-Type Semiconductors: Challenges and Opportunities. *Acc. Chem. Res.* **2010**, *43*, 1063−1071.
(38) Scherer, M. R. J.; Steiner, U. Efficient Electrochromic Devices Made from 3D Nanotubular Gyroid Networks. *Nano Lett.* **2013**, *13*, 3005−3010.
(39) Sialvi, M. Z.; Mortimer, R. J.; Wilcox, G. D.; Teridi, A. M.; Varley, T. S.; Wijayantha, K. G. U.; Kirk, C. a. Electrochromic and Colorimetric Properties of Nickel(II) Oxide Thin Films Prepared by Aerosol-Assisted Chemical Vapor Deposition. *ACS Appl. Mater. Interfaces* **2013**, *5*, 5675−5682.
(40) Trotochaud, L.; Ranney, J. K.; Williams, K. N.; Boettcher, S. W. Solution-Cast Metal Oxide Thin Film Electrocatalysts for Oxygen Evolution. *J. Am. Chem. Soc.* **2012**, *134*, 17253−17261.
(41) Suntivich, J.; May, K. J.; Gasteiger, H. A.; Goodenough, J. B.; Shao-Horn, Y. A Perovskite Oxide Optimized for Oxygen Evolution Catalysis from Molecular Orbital Principles. *Science* **2011**, *334*, 1383−1385.
(42) Lyons, M. E. G.; Russell, L.; O'Brien, M.; Doyle, R. L.; Godwin, I.; Brandon, M. P. Redox Switching and Oxygen Evolution at Hydrous Oxyhydroxide Modified Nickel Electrodes in Aqueous Alkaline Solution: Effect of Hydrous Oxide Thickness and Base Concentration. *Int. J. Electrochem. Sci.* **2012**, *7*, 2710−2763.
(43) Fletcher, S. Tafel Slopes from First Principles. *J. Solid State Electrochem.* **2008**, *13*, 537−549.
(44) A 120 mV/decade Tafel slope indicates that the rate-limiting step is the first step and is electronic. A 60 mV/decade Tafel slope indicates that the rate-limiting step is chemical (e.g., proton transfer) and is proceeding via an electron transfer step. A 40 mV/decade Tafel slope indicates that the rate-limiting step is electron transfer and is the second step in the catalysis. A 30 mV/decade Tafel slope indicates that the rate-limiting step is the second step and is necessarily chemical (i.e., proton transfer) and proceeding via an electron transfer step.
(45) Godwin, I. J.; Lyons, M. E. G. Enhanced Oxygen Evolution at Hydrous Nickel Oxide Electrodes Via Electrochemical Ageing in Alkaline Solution. *Electrochem. Commun.* **2013**, *32*, 39−42.
(46) Lyons, M. E. G.; Brandon, M. P. The Oxygen Evolution Reaction on Passive Oxide Covered Transition Metal Electrodes in Aqueous Alkaline Solution. Part 1—Nickel. *Int. J. Electrochem. Sci.* **2008**, *3*, 1386−1424.
(47) In our hands, the observed Tafel slope is dependent on electrode conditioning; when the electrode is conditioned for an hour at 1.5 V vs Ag/AgCl in sat KCl, a Tafel slope of 40 mV/decade is observed between 0.5 V and 0.8 V.